The inactive Dnmt3b3 isoform preferentially enhances Dnmt3b-mediated DNA methylation

Yang Zeng,[1,2,3,4] Ren Ren,[1,2,4] Gundeep Kaur,[1,2,4] Swanand Hardikar,[1,2] Zhengzhou Ying,[1,2] Lance Babcock,[1,2] Esha Gupta,[1,2] Xing Zhang,[1,2] Taiping Chen,[1,2] and Xiaodong Cheng[1,2]

[1]Department of Epigenetics and Molecular Carcinogenesis, [2]Center for Cancer Epigenetics, The University of Texas MD Anderson Cancer Center, Houston, Texas 77030, USA; [3]Program in Genetics and Epigenetics, The University of Texas MD Anderson Cancer Center UTHealth Graduate School of Biomedical Sciences, Houston, Texas 77030, USA

The de novo DNA methyltransferases Dnmt3a and Dnmt3b play crucial roles in developmental and cellular processes. Their enzymatic activities are stimulated by a regulatory protein Dnmt3L (Dnmt3-like) in vitro. However, genetic evidence indicates that Dnmt3L functions predominantly as a regulator of Dnmt3a in germ cells. How Dnmt3a and Dnmt3b activities are regulated during embryonic development and in somatic cells remains largely unknown. Here we show that Dnmt3b3, a catalytically inactive Dnmt3b isoform expressed in differentiated cells, positively regulates de novo methylation by Dnmt3a and Dnmt3b with a preference for Dnmt3b. Dnmt3b3 is equally potent as Dnmt3L in stimulating the activities of Dnmt3a2 and Dnmt3b2 in vitro. Like Dnmt3L, Dnmt3b3 forms a complex with Dnmt3a2 with a stoichiometry of 2:2. However, rescue experiments in *Dnmt3a/3b/3l* triple-knockout (TKO) mouse embryonic stem cells (mESCs) reveal that Dnmt3b3 prefers Dnmt3b2 over Dnmt3a2 in remethylating genomic sequences. Dnmt3a2, an active isoform that lacks the N-terminal uncharacterized region of Dnmt3a1 including a nuclear localization signal, has very low activity in TKO mESCs, indicating that an accessory protein is absolutely required for its function. Our results suggest that Dnmt3b3 and perhaps similar Dnmt3b isoforms facilitate de novo DNA methylation during embryonic development and in somatic cells.

[*Keywords*: DNA cytosine methylation; Dnmt3a; Dnmt3b; Dnmt3b3; de novo methylation]

Supplemental material is available for this article.

Received June 23, 2020; revised version accepted August 27, 2020.

In mammals and other vertebrates, DNA methylation occurs at the C5 position of cytosine, generating 5-methylcytosine (5mC), mostly within CpG dinucleotides. This methylation, together with histone modifications, plays an important role in modulating chromatin structure, thus controlling gene expression and many other chromatin-dependent processes (for review, see Bestor 2000; Goll and Bestor 2005; Jones and Liang 2009; Cheng and Blumenthal 2010; Li and Zhang 2014; Lyko 2018). The resulting epigenetic effects maintain the various patterns of gene expression in different cell types (for reviews, see Jones and Baylin 2002; De Carvalho et al. 2010; Abyzov and Vaccarino 2020; Ferrer et al. 2020; Westerman and Ordovás 2020). In mammals, DNA methyltransferases (Dnmts) include three proteins, belonging to two families that are structurally and functionally distinct. Dnmt3a and Dnmt3b establish the initial CpG methylation pattern de novo, while Dnmt1 maintains faithfully this pattern during DNA replication.

The Dnmt3 family includes two active de novo enzymes, Dnmt3a and Dnmt3b, and one regulatory factor, Dnmt3-like (Dnmt3L) (Fig. 1A; Goll and Bestor 2005). Dnmt3a and Dnmt3b have similar domain arrangements: Both contain a variable region at the N terminus, followed by a PWWP domain, which has been implicated in nonspecific DNA binding (Qiu et al. 2002), heterochromatin localization (Chen et al. 2004), and histone H3K36me2/3 binding (Dhayalan et al. 2010; Weinberg et al. 2019); a Cys-rich 3-Zn-binding ATRX-Dnmt3-Dnmt3L (ADD) domain; and a C-terminal catalytic domain. The amino acid sequence of Dnmt3L is very similar to that of Dnmt3a and Dnmt3b in the ADD domain that specifically interacts with unmethylated lysine 4 of histone H3 (H3K4me0) (Ooi et al. 2007; Otani et al. 2009), but it lacks a PWWP domain and suffers three deletions in the

[4]**These authors contributed equally to this work.**
Corresponding authors: xcheng5@mdanderson.org, tchen2@mdanderson.org

Article published online ahead of print. Article and publication date are online at http://www.genesdev.org/cgi/doi/10.1101/gad.341925.120. Freely available online through the *Genes & Development* Open Access option.

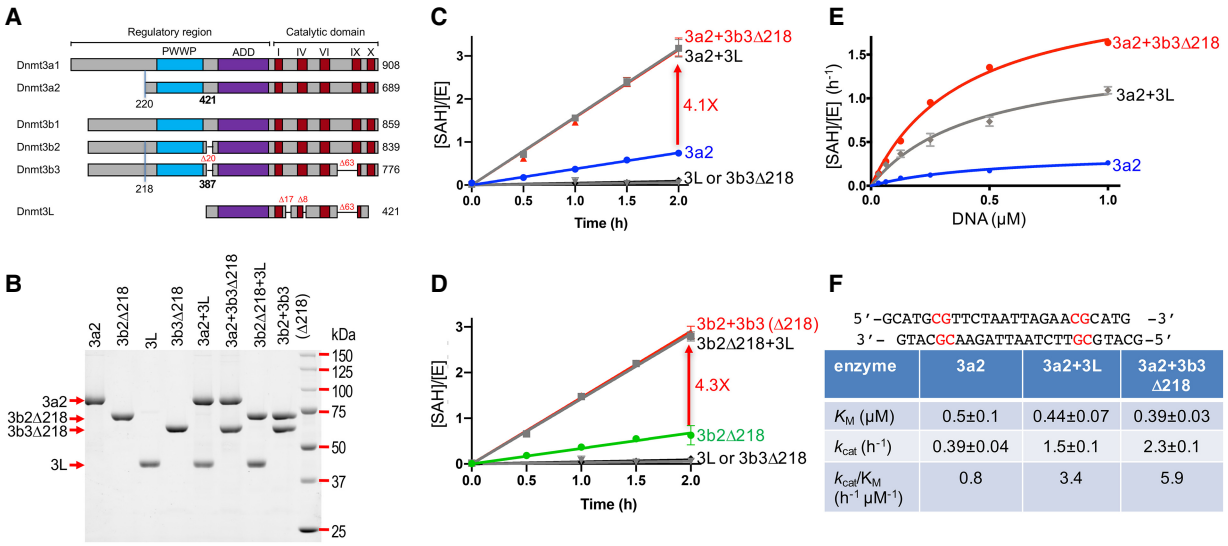

enzyme	3a2	3a2+3L	3a2+3b3 Δ218
K_M (μM)	0.5±0.1	0.44±0.07	0.39±0.03
k_{cat} (h^{-1})	0.39±0.04	1.5±0.1	2.3±0.1
k_{cat}/K_M (h^{-1} μM^{-1})	0.8	3.4	5.9

Figure 1. Dnmt3b3Δ218 stimulates Dnmt3a2 and 3b2Δ218 activities. (*A*) Members of mouse Dnmt3 family. The N termini of the Dnmt3a2, 3b2, and 3b3 used in the study are indicated. (*B*) Examples of purified recombinant enzymes used in the activity assays, shown in a 12% PAGE with Bio-Rad stain-free image. (*C*,*D*) Activities of Dnmt3a2 and 3b2Δ218 in the absence and presence of 3L or 3b3Δ218. (*E*,*F*) Kinetics of Dnmt3a2 in the absence and presence of 3L and 3b3Δ218.

C-terminal domain that lose residues for SAM binding (Δ17), the catalytic loop including a proline–cysteine (PC) motif (Δ8), and the target recognition DNA-binding domain (Δ63) (Supplemental Fig. S1A,B). However, Dnmt3L retains an overall fold of classic class-I methyltransferase (Ooi et al. 2007).

While Dnmt3L is capable of interacting with both Dnmt3a and Dnmt3b and stimulating their activities in vitro (Chedin et al. 2002; Suetake et al. 2004; Chen et al. 2005; Gowher et al. 2005; Kareta et al. 2006), genetic evidence suggests that Dnmt3L mainly regulates Dnmt3a activity and functions in vivo. Specifically, *Dnmt3l* knockout (KO) mice exhibit a germline phenotype that is indistinguishable from that of *Dnmt3a* germ cell-specific conditional KO mice—both fail to undergo de novo DNA methylation, including the establishment of genomic imprinting (Bourc'his et al. 2001; Hata et al. 2002; Bourc'his and Bestor 2004; Kaneda et al. 2004; Webster et al. 2005). However, *Dnmt3l* KO mice, apart from being infertile, are grossly normal (Bourc/'his et al. 2001; Hata et al. 2002), unlike *Dnmt3b* KO mice, which are embryonically lethal (Okano et al. 1999). These results indicate that Dnmt3L functions primarily as an accessory factor of Dnmt3a in the germline, but is dispensable for de novo methylation during embryogenesis, which is mainly catalyzed by Dnmt3b (Okano et al. 1999; Bourc'his et al. 2001; Hata et al. '2002; Kaneda et al. 2004; Borgel et al. 2010).

Dnmt3L and Dnmt3a interact through their C-terminal domains (Jia et al. 2007). This complex contains two monomers each of Dnmt3a and Dnmt3L, forming a tetramer with two 3L-3a interfaces and one 3a-3a interface (3L-3a-3a-3L) (Jia et al. 2007; Guo et al. 2015; Zhang et al. 2018). Substituting key, although noncatalytic, residues at the Dnmt3a-3L or Dnmt3a-3a interfaces eliminates enzymatic activity, indicating that both interfaces are essential for catalysis (Jia et al. 2007). This has led to a model in which Dnmt3L binds to H3K4me0 (via its ADD domain) and recruits, stabilizes, and stimulates Dnmt3a activity to regions of chromatin where H3K4 is unmethylated. Such a model could explain part of the puzzle of how DNA methylation patterns are established de novo in developing germ cells, which express high levels of Dnmt3L and Dnmt3a2, a Dnmt3a isoform that lacks the N-terminal region of Dnmt3a1 (Supplemental Fig. S1A; Chen et al. 2002). Although Dnmt3L is also expressed and may be involved in de novo methylation in early embryos and mESCs (Guenatri et al. 2013; Veland et al. 2019), it is not essential for embryonic development (Bourc'his et al. 2001; Hata et al. 2002), suggesting the possible involvement of additional regulators of de novo methylation. Furthermore, whereas Dnmt3a and 3b expression is retained throughout development and in somatic cells, Dnmt3L is quickly silenced upon differentiation (Hata et al. 2002; Guenatri et al. 2013). This raises the question of how de novo DNA methylation is regulated during embryonic development and in somatic cells; i.e., what is the molecular basis of Dnmt3L-independent regulation?

In contrast to *Dnmt3a*, which produces two major active isoforms, Dnmt3a1 and Dnmt3a2, due to transcription driven by different promoters (Okano et al. 1998; Chen et al. 2002), *Dnmt3b* produces a large number of splice variants (over 30 have been reported), many of which are catalytically inactive. Among the relatively more abundant Dnmt3b1–Dnmt3b8 (Supplemental Fig. S1A; Okano et al. 1998; Robertson et al. 1999; Chen et al. 2002; Weisenberger et al. 2004), Dnmt3b1 and Dnmt3b2 have an intact C-terminal catalytic domain and are enzymatically active, while Dnmt3b3-8 have deletions in the C-terminal domain (due to exclusion of exon 21 and/or exon 22) and are predicted to be inactive.

Dnmt3b2-5 have an additional 20-residue deletion between the PWWP and ADD domains (due to exclusion of exon 10). Most interestingly, Dnmt3b3, which is expressed in normal somatic cells (Chen et al. 2002; Weisenberger et al. 2004), and Dnmt3b6, which is expressed in mESCs (Chen et al. 2002), have the exact 63-residue deletion corresponding to that of Dnmt3L (Supplemental Fig. S1A,B). Indeed, previous studies indicated that catalytically inactive Dnmt3b isoforms could positively or negatively modulate DNA methylation in cancer cell lines (Saito et al. 2002; Weisenberger et al. 2004; Wang et al. 2007; Ostler et al. 2012; Duymich et al. 2016), suggesting that they may function as DNA methylation regulators. However, the molecular mechanisms by which inactive Dnmt3b isoforms regulate DNA methylation and their functional specificities remain elusive.

In this study, we demonstrated that Dnmt3b3 alone is inactive in vitro but stimulates the catalytic activity of Dnmt3a2 and Dnmt3b2 and that the optimal stimulation is reached at equal molar stoichiometry. Rescue experiments in *Dnmt3a/3b/3l* triple-KO (TKO) mESCs revealed that Dnmt3b3 strongly enhances Dnmt3b2-mediated DNA methylation and only modestly enhances Dnmt3a1- or Dnmt3a2-mediated DNA methylation. The stimulatory effect of Dnmt3b3 is dependent on its ability to interact with active Dnmt3a/3b proteins. We also showed that the presence of an accessory protein (e.g., Dnmt3L and Dnmt3b3) is absolutely required for Dnmt3a2 activity in mESCs and identified a nuclear localization signal (NLS) in the N-terminal region of Dnmt3a1 that contributes to its function. As Dnmt3b3 is ubiquitously expressed in differentiated cells (Chen et al. 2002; Weisenberger et al. 2004) and Dnmt3b6, another Dnmt3b isoform similar to Dnmt3b3 (Supplemental Fig. S1A), is highly expressed in early embryos and mESCs (Chen et al. 2002), we propose that these inactive Dnmt3b proteins serve as accessory factors of Dnmt3b, and perhaps Dnmt3a1 as well, in facilitating de novo methylation during embryonic development and in somatic cells, similar to the role of Dnmt3L in assisting Dnmt3a2 in germ cells.

Results

Dnmt3b3, an inactive isoform, stimulates activities of Dnmt3a and Dnmt3b in vitro

We generated a series of constructs of mouse Dnmt3a and Dnmt3b (Supplemental Table S1) that included the full length Dnmt3a2, which is produced from an alternative promoter resulting in lacking the first 219 residues of Dnmt3a1 (Chen et al. 2002), Dnmt3b2Δ218, a N-terminal truncated Dnmt3b2 equivalent to that of Dnmt3a2 (Qiu et al. 2002), and corresponding Dnmt3b3Δ218 (Fig. 1A). All constructs were expressed in *E. coli* and individual enzymes (3a2 and 3b2Δ218) or their complexes with Dnmt3L or 3b3Δ218 were purified to near homogeneity (Fig. 1B).

A close examination of Dnmt3b splice variants (Supplemental Fig. S1) revealed that Dnmt3b3 and 3b6 share the exact deletion of the 63 residues in the C-terminal domain (Supplemental Fig. S1B). Although retaining the residues for SAM binding and catalysis, Dnmt3b3Δ218 is inactive (like Dnmt3L), whereas Dnmt3a2 and 3b2Δ218 have comparable in vitro activities (Fig. 1C,D) on a DNA oligonucleotide containing two CpG sites (Jia et al. 2007; Zhang et al. 2018).

To investigate whether Dnmt3b3 can stimulate the enzymatic activities of Dnmt3a and Dnmt3b, we first repeated the reported data that Dnmt3L stimulates DNA methylation activities of Dnmt3a and Dnmt3b. We found that the activities of 3a2 and 3b2Δ218 are stimulated by a factor of ∼4 in the presence of Dnmt3L (Fig. 1C,D), in agreement with previous findings (Chedin et al. 2002; Suetake et al. 2004; Gowher et al. 2005). Under the same reaction conditions established for Dnmt3a2-3L complex, we measured the activities of 3a2 and 3b2Δ218 in the presence of 3b3Δ218, which stimulated the activities of 3a2 and 3b2Δ218 to the same magnitude (Fig. 1C,1D). The gain in Dnmt3a2 catalytic efficiency by the presence of 3L or 3b3Δ218 is driven largely by an improved reaction in k_{cat} (3.8× for 3a2-3L and 5.9× for 3a2-3b3 Δ218) without affecting binding of DNA substrate (K_m values varied from 0.5 to 0.4 μM) (Fig. 1E,F). For Dnmt3b2Δ218, the values K_m and k_{cat} are both increased (Supplemental Fig. S1C,D).

Dnmt3a2 and 3b3Δ218 form a stable complex

Because most structural studies so far used the C-terminal fragments of Dnmt3a and Dnmt3L (Jia et al. 2007; Guo et al. 2015; Zhang et al. 2018; Anteneh et al. 2020), except for recent work on Dnmt3B-Dnm3L (Gao et al. 2020; Lin et al. 2020), we focused our biophysical work on the complex between Dnmt3a2 and Dnmt3b3. First, we used three biophysical methods to measure the absolute mass of the complex of 3a2-3b3Δ218. The protein samples at two different concentrations (5 and 10 mg/mL) were subjected to size-exclusion chromatography coupled with multiangle light scattering (Some et al. 2019), which gave the absolute mass of 312–316 kDa (Fig. 2A; Supplemental Fig. S2). The same fractions eluted from the size exclusion chromatography were simultaneously examined by synchrotron small-angle X-ray scattering (SAXS) (Kikhney and Svergun 2015), which gave the molecular weight of 293–302 kDa and the maximum dimension of the complex to be ∼180–185 Å long (Fig. 2A; Supplemental Fig. S3). Finally, sedimentation velocity analytical ultracentrifugation studies revealed the presence of three populations: the major peak at 295 kDa (in agreement with the two scattering methods), a second peak at 72 kDa, and a minor peak at 161 kDa (Fig. 2B). The observed molecular mass at ∼300 kDa agrees well with the calculated mass of Dnmt3a2 and 3b3Δ218 forming a complex with a stoichiometry of 2:2 (Fig. 2A). The lower-molecular-weight peaks reflected samples degradation during the AUC experiment, which lasted overnight (data not shown).

The overall shape of the SAXS envelopes (Fig. 2C; Supplemental Fig. S3) agrees with negative stain electron microscopy (EM) models (Fig. 2D; Supplemental Fig. S4). We generated negative stain EM models for the three complexes with increased protein sizes: the C-terminal

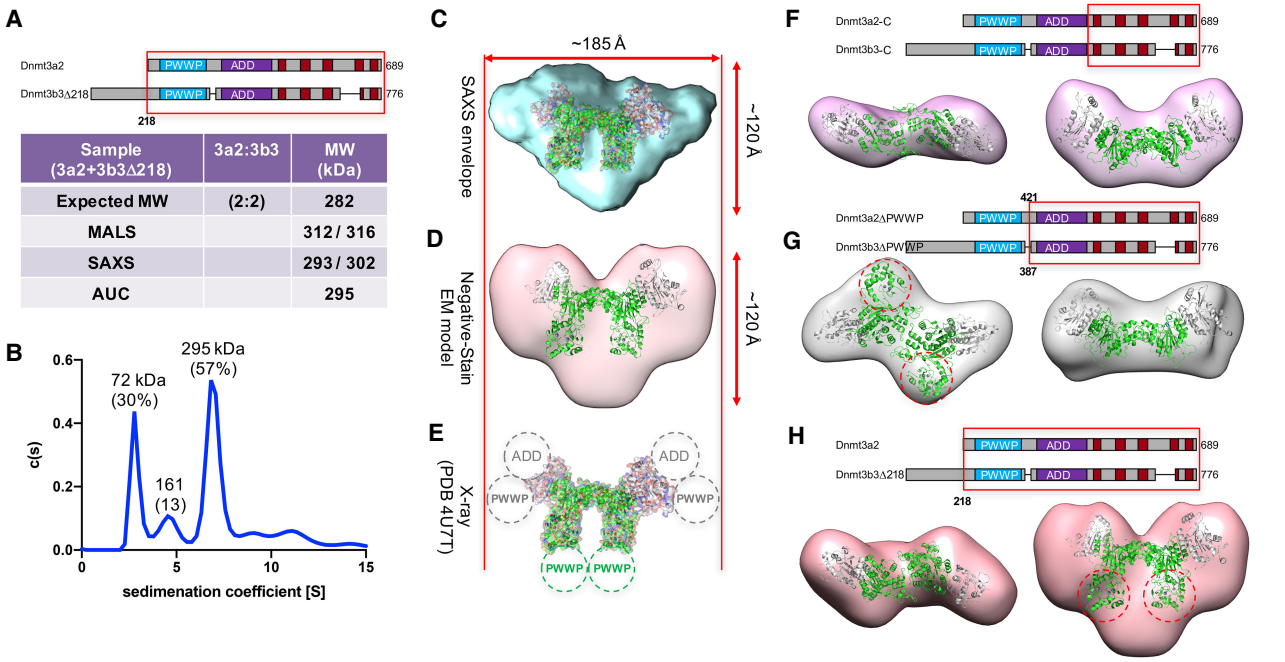

Figure 2. Dnmt3a2 and 3b3Δ218 form a stable complex. (*A*) Summary of mass measurements by three biophysical methods. (*B*) Sedimentation coefficient distribution profile. (*C*) The SAXS envelope (Supplemental Fig. S3). (*D*) The negative stain EM model (Supplemental Fig. S4). (*E*) X-ray structure of Dnmt3a fragment containing ADD and C-terminal methyltransferase domain (in green) and Dnmt3L C-terminal methyltransferase-like domain (in gray) (PDB 4U7T) (Guo et al. 2015). The additional domains used in the SAXS and EM studies are indicated by the dashed circles. (*F–H*) Three negative stain EM models of Dnmt3a2-3b3 with increased protein size. (*F*) The C-terminal minimal domains, with docked X-ray structure (PDB 2QRV). (*G*) The ADD-methyltransferase fragments, with docked X-ray structure (PDB 4U7P) where two ADDs of Dnmt3a (green) are in an open conformation. (*H*) The PWWP-ADD-methyltransferase fragments, with docked X-ray structure (PDB 4U7T) where ADDs are in a closed conformation.

minimal domains of Dnmt3a and Dnmt3b3 (Fig. 2F), the fragments containing ADD domain (Fig. 2G), and the fragments containing both PWWP and ADD domains (Fig. 2H). The overall contour of the minimal C-terminal domain is elongated with an indentation of the density in the middle, which can be easily docked with the butterfly shaped tetramer structure of 3L-3a-3a-3L (PDB 2QRV). The concavity of the density in the middle of the surface is also noticeable in the two larger complexes, which guided the docking of the available X-ray structure of Dnmt3a (containing the ADD and methyltransferase domains) and Dnmt3L (containing the C-terminal methyltransferase-like domain) (Guo et al. 2015). The ADD domain of Dnmt3a has been observed in two different conformations in the previous structural characterization (Guo et al. 2015): an open conformation (PDB 4T7P) and a closed conformation (PDB 4U7T). In the absence of the N-terminal PWWP domain (Dnmt3a2-3b3 ΔPWWP construct), the EM model can be fitted with the open conformation of the two copies of the ADD domain of Dnmt3a in opposite directions (red circles in Fig. 2G). In the presence of the N-terminal PWWP domain, the two copies of the ADD domain of Dnmt3a are restrained to the closed conformation (the red circles in Fig. 2H). In addition, we observed unaccounted density near the bottom as well as the two sides of the envelope (Fig. 2H). We assume these additional densities might be the location where the missing four copies of PWWP from both proteins and two copies of ADD of Dnmt3b3 (Fig. 2E). The relative positions of the four copies PWWP and ADD domains in respect to the two catalytic domains might undergo conformational changes upon binding nucleosome substrate. Interestingly, in a very recently determined cryo-EM structure of Dnmt3a2-3b3 bound with nucleosome, the ADD and PWWP domains are all disordered (PDB 6PA7) (Xu et al. 2020).

Dnmt3b3 can substitute Dnmt3L in mESCs in stimulating de novo DNA methylation with a preference for Dnmt3b

To assess the role of Dnmt3b3 in stimulating Dnmt3a and Dnmt3b in vivo, we first performed rescue experiments in *Dnmt3a/3b* double-knockout (DKO) mESCs (Okano et al. 1999). These cells, after prolonged culture, exhibit severe loss of global DNA methylation, and genomic sequences can be redundantly or preferentially remethylated by exogenously expressed Dnmt3a and Dnmt3b enzymes (Chen et al. 2003). We established stable clones in DKO mESCs expressing Myc-tagged Dnmt3a2 or Dnmt3b2 and FLAG-tagged Dnmt3b3 or GFP (control) simultaneously from a single plasmid vector using the "self-cleaving" P2A peptide (Supplemental Fig. S5A,B; Kim et al. 2013). The methylation levels of pericentromeric major satellite repeats

and centromeric minor satellite repeats, which are preferentially methylated by Dnmt3a and Dnmt3b, respectively (Chen et al. 2003), were analyzed by Southern blot following digestion of genomic DNA with methylation-sensitive restriction enzymes. As expected, expression of Dnmt3a2 or Dnmt3b2 resulted in almost complete or partial recovery of DNA methylation levels at the major and minor satellite repeats according to their target preferences. However, coexpression of Dnmt3b3 (compared with GFP) showed little effect on the remethylation activities of Dnmt3a2 and Dnmt3b2 (Supplemental Fig. S5C). We reasoned that the presence of Dnmt3L in DKO mESCs might have "masked" the effect of Dnmt3b3.

Next, we repeated the rescue experiments in *Dnmt3a/3b/3l* TKO mESCs, which were generated by disrupting *Dnmt3l* in *Dnmt3a/3b* DKO cells using the CRISPR/Cas9 gene editing technology (Supplemental Fig. S6). Using the same strategy as described above, we established stable clones in TKO mESCs coexpressing Myc-tagged Dnmt3a2 or Dnmt3b2 and FLAG-tagged Dnmt3b3, GFP (negative control) or Dnmt3L (positive control). For each vector, two clones, a high expressor and a low expressor, were selected for subsequent experiments, with the high or low expressors of all vectors showing similar levels of Myc-Dnmt3a2 or Myc-Dnmt3b2. Immunoblotting with Dnmt3a, Dnmt3b, and Dnmt3L antibodies indicated that the low expressors had <10% and the high expressors had ~30%–50% of endogenous Dnmt3a2, Dnmt3b, and Dnmt3L levels in wild-type (WT) mESCs (Fig. 3A). Southern blot analysis revealed that Dnmt3a2 alone (i.e., Dnmt3a2 + GFP) had no detectible activity, while Dnmt3b2 alone (i.e., Dnmt3b2 + GFP) showed moderate activity, in remethylating major and minor satellite DNA. Dnmt3b3 enhanced DNA methylation by both

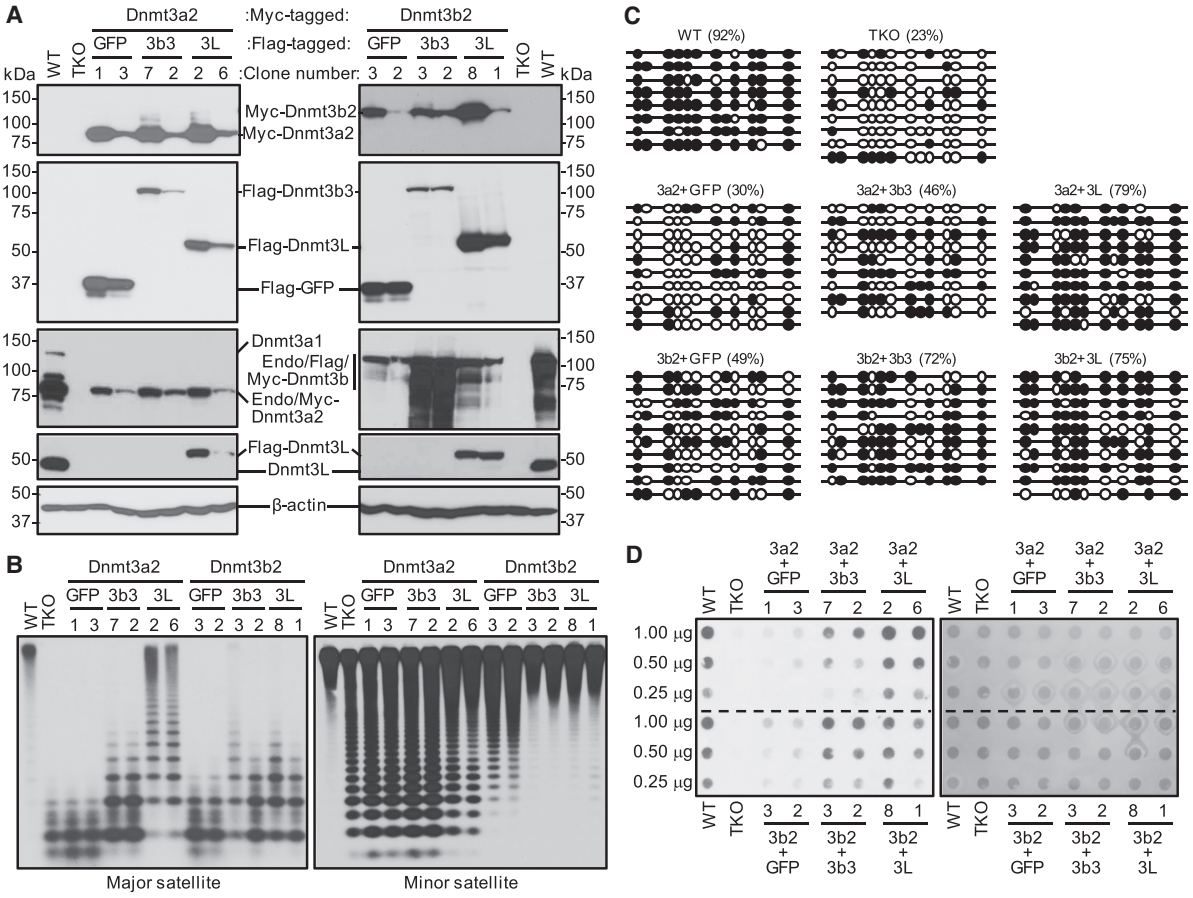

Figure 3. Dnmt3b3 enhances Dnmt3a2- or Dnmt3b2-mediated DNA methylation in *Dnmt3a/3b/3l* TKO mESCs. (*A*) Western blots showing the expression of Myc- and FLAG-tagged proteins in stable clones established in *Dnmt3a/3b/3l* TKO mESCs. Shown from *top* to *bottom* are blots with Myc, FLAG, Dnmt3a (*left* panel) or Dnmt3b (*right* panel), Dnmt3L, and β-actin antibodies. Note that FLAG-Dnmt3b3 yields higher background in the Dnmt3b blot. Endo, endogenous. (*B*) Southern blot analysis of the major and minor satellite repeats after digestion of genomic DNA with methylation-sensitive restriction enzymes (MaeII for major satellite; HpaII for minor satellite). (*C*) Bisulfite sequencing analysis showing methylation levels at IAP retrotransposons. Note that the amplified region has eight to 12 CpG sites due to sequence variations. Unmethylated and methylated CpG sites are shown as open and filled circles, respectively. The methylation percentages are indicated. (*D*) Dot blot analysis with 5mC antibody (*left* panel) and total DNA (*right* panel) in clones of Myc-Dnmt3a2 (*top* half) or Myc-Dnmt3b2 (*bottom* half). (*Right*) The same membrane was stained with SYTOX Green to verify DNA loading. For each DNA sample, three amounts (1 µg, 0.5 µg, and 0.25 µg) were examined.

Dnmt3a2 and Dnmt3b2, with its effect being as potent as that of Dnmt3L on Dnmt3b2 and substantially less potent than that of Dnmt3L on Dnmt3a2 (Fig. 3B). Notably, the high- and low-expressing clones of each vector had similar levels of methylation at the favored target (i.e., major satellite for Dnmt3a2 and minor satellite for Dnmt3b2), although they appeared to show "dose effects" at the disfavored target (i.e., the high Dnmt3b2-expressing clone had modestly higher methylation level at major satellite than the low-expressing counterpart) (Fig. 3B). This suggests that the different effects of Dnmt3b3 and Dnmt3L on Dnmt3a2 activity are due to intrinsic differences of the Dnmt3a2-3b3 and Dnmt3a2-3L complexes rather than differences in protein expression levels.

To rule out biased effects on specific genomic regions, we performed bisulfite sequencing analysis of the methylation levels at intracisternal A particle (IAP) retrotransposons (Fig. 3C), which are redundantly methylated by Dnmt3a and Dnmt3b (Chen et al. 2003), and analyzed total 5mC levels by dot blot with a 5mC antibody (Fig. 3D). The data demonstrated that Dnmt3a2 alone (Dnmt3a2 + GFP) had very low activity and confirmed that Dnmt3b3 preferred Dnmt3b2 over Dnmt3a2, whereas Dnmt3L showed robust effects on both Dnmt3a2 and Dnmt3b2 (Fig. 3C,D). In summary, we demonstrate that Dnmt3b3 strongly stimulates Dnmt3b2 and modestly stimulates Dnmt3a2 in cells deficient for Dnmt3L.

The ability of Dnmt3b3 to interact with active Dnmt3 proteins is required for its stimulating effect

Dnmt3L interacts with Dnmt3a to form a tetramer of 3L-3a-3a-3L (Jia et al. 2007; Guo et al. 2015; Zhang et al. 2018). Our biophysical data suggest that Dnm3a2 and Dnmt3b3Δ218 also form a complex with a stoichiometry of 2:2 (Fig. 2). To determine whether the ability of Dnmt3b3 to interact with Dnmt3a2 and Dnmt3b2 is important for its stimulating effect, we substituted phenylalanine 659 in Dnmt3b3 with aspartate (F659D) (Fig. 4A). F659 in Dnmt3b3 is a conserved residue in the Dnmt3 family that corresponds to F297 in Dnmt3L at the Dnmt3L-3a interface (Supplemental Fig. S1B; Jia et al. 2007). By coimmunoprecipitation (co-IP) experiments using Myc-tagged Dnmt3a2 or Dnmt3b2 and HA-tagged Dnmt3b3 proteins transiently expressed in HEK293 cells or *Dnmt3a/3b/3l* TKO mESCs, we confirmed that WT Dnmt3b3 interacted with Dnmt3a2 and Dnmt3b2 and that the F659D substitution disrupted the interactions (Fig. 4B). Unlike WT Dnmt3b3, the F659D variant, when coexpressed with Dnmt3a2 or Dnmt3b2 in stable clones established in TKO mESCs (Fig. 4C), failed to enhance remethylation of major and minor satellite DNA by the active enzymes (Fig. 4D). These results further suggest that the mechanism by which Dnmt3b3 stimulates active Dnmt3a/3b proteins is similar to that of Dnmt3L.

Dnmt3a1 harbors an N-terminal nuclear localization signal that contributes to its function

In contrast to its dramatic activity in *Dnmt3a/3b* DKO mESCs (Supplemental Fig. S5; Chen et al. 2003), Dnmt3a2 showed little activity in *Dnmt3a/3b/3l* TKO mESCs (Fig. 3), indicating that an accessory factor is important for Dnmt3a2 activity in cells. We asked whether Dnmt3a1, which is equally active as Dnmt3a2 in DKO mESCs (Chen et al. 2003), would also behave like Dnmt3a2 in TKO mESCs. Rescue experiments showed that, unlike Dnmt3a2 but similar to Dnmt3b2 (Fig. 3), Dnmt3a1 alone

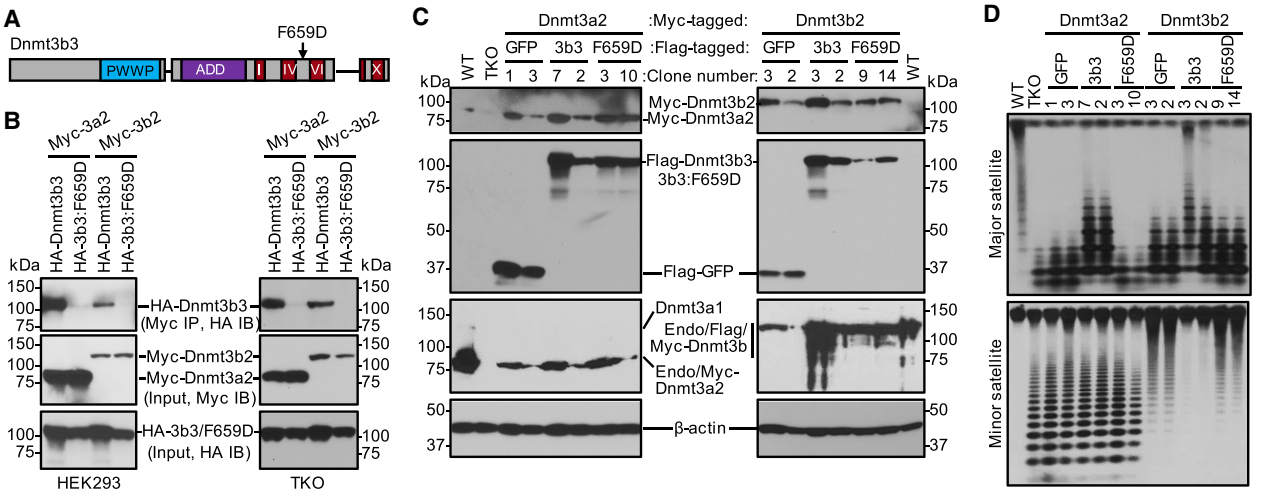

Figure 4. Dnmt3b3 F659D substitution fails to stimulate Dnmt3a2 and Dnmt3b2. (*A*) Location of the F659D mutation in Dnmt3b3. (*B*) Co-IP assay showing that HA-tagged Dnmt3b3, but not the F659D mutant, interacts with Myc-Dnmt3a2 and Myc-Dnmt3b2 when coexpressed in HEK293 cells (*left* panel) or *Dnmt3a/3b/3l* TKO mESCs (*right* panel). (IP) Immunoprecipitates, (IB) immunoblotting, (Input) total cell lysate. (*C*) Western blots showing the expression of Myc- and FLAG-tagged proteins in stable clones established in *Dnmt3a/3b/3L* TKO mESCs. Shown from *top* to *bottom* are blots with Myc, FLAG, Dnmt3a (*left* panel) or Dnmt3b (*right* panel), and β-actin antibodies. (Endo) Endogenous. (*D*) Southern blot analysis of the major and minor satellite repeats showing that the Dnmt3b3 F659D mutant fails to enhance Dnmt3a2- or Dnmt3b2-mediated DNA methylation.

(i.e., Dnmt3a1+GFP) induced moderate remethylation of major and minor satellite DNA. Its activity could be strongly and slightly enhanced by Dnmt3L and Dnmt3b3, respectively (Fig. 5A,B).

The two Dnmt3a isoforms differ in the N-terminal unstructured region in Dnmt3a1 (219 residues in mice and 223 residues in humans) being absent in Dnmt3a2 (Fig. 1A; Chen et al. 2002). Because these isoforms are equally active in in vitro assays and in rescue experiments in *Dnmt3a/3b* DKO mESCs (Chen et al. 2002, 2003), the N-terminal region of Dnmt3a1 has not been well characterized. Our observation that Dnmt3a1 is substantially more active than Dnmt3a2 in *Dnmt3a/3b/3l* TKO mESCs indicates that the extra N-terminal region is functionally important. We examined the localization of Dnmt3a1 and Dnmt3a2 by transiently expressing GFP-Dnmt3a1 or GFP-Dnmt3a2 in NIH3T3 cells (Fig. 5C). As reported previously (Chen et al. 2002), Dnmt3a1 localized exclusively in the nuclei and largely concentrated in heterochromatin foci, whereas Dnmt3a2 localized in both the nuclei and cytoplasm with an obvious enrichment and diffused pattern in the nuclei except the nucleoli (Fig. 5D). A GFP fusion protein with only the N-terminal 219 amino acids (GFP-3a-N, Fig. 5C) localized entirely in the nuclei with a diffused pattern excluding the nucleoli (Fig. 5D). The region contains two arginine/lysine (RK)-rich sequences (residues 43–53 and residues 196–215) that are conserved in human and mouse Dnmt3a1. A fragment containing residues 43–53 (i.e., GFP-3a [1–118]) (Fig. 5C) showed a diffused pattern throughout the cell, like GFP alone, whereas a fragment containing residues 196–215 (i.e., GFP-3a [119–219]) (Fig. 5C) displayed a nuclear localization pattern identical to that of GFP-Dnmt3a-N (Fig. 5D). Indeed, part of the sequence, 198-KRDEWLARWKREAEKKAK-215, conforms perfectly to the consensus sequence of the bipartite NLS: (K/R)(K/R)X10–12(K/R)3/5 (Kosugi et al. 2009). Thus, we conclude that this sequence is a functional NLS that contributes to the exclusive localization of Dnmt3a1 to the nuclei. In contrast, a GFP fusion protein with the N-terminal 178 amino acids of Dnmt3b localized in both the nuclei and cytoplasm of transfected NIH 3T3 cells with nuclear enrichment (Supplemental Fig. S7). Thus, the N-terminal region of Dnmt3b likely contributes to, but is not sufficient for, nuclear localization of Dnmt3b proteins (Chen et al. 2004).

Discussion

Dnmt3a and Dnmt3b show low enzymatic activities in vitro but are robust in carrying out de novo DNA methylation during development, suggesting the involvement of critical regulatory factors in vivo. In this study, we demonstrate that Dnmt3b3, a catalytically inactive Dnmt3b isoform, positively regulates de novo methylation by preferentially stimulating Dnmt3b activity in mESCs deficient for Dnmt3L. We also show that Dnmt3a2, the predominant Dnmt3a isoform in germ cells and mESCs (Chen et al. 2002; Sakai et al. 2004), has very low activity in *Dnmt3a/3b/3l* TKO mESCs, and its activity can be strongly and modestly enhanced by Dnmt3L and Dnmt3b3, respectively. Our results support a model that, while Dnmt3L serves as a key accessory factor of Dnmt3a2 in germ cells, Dnmt3b3 and perhaps other inactive Dnmt3b isoforms (e.g., Dnmt3b6) play important roles in facilitating de novo methylation by Dnmt3b, and perhaps

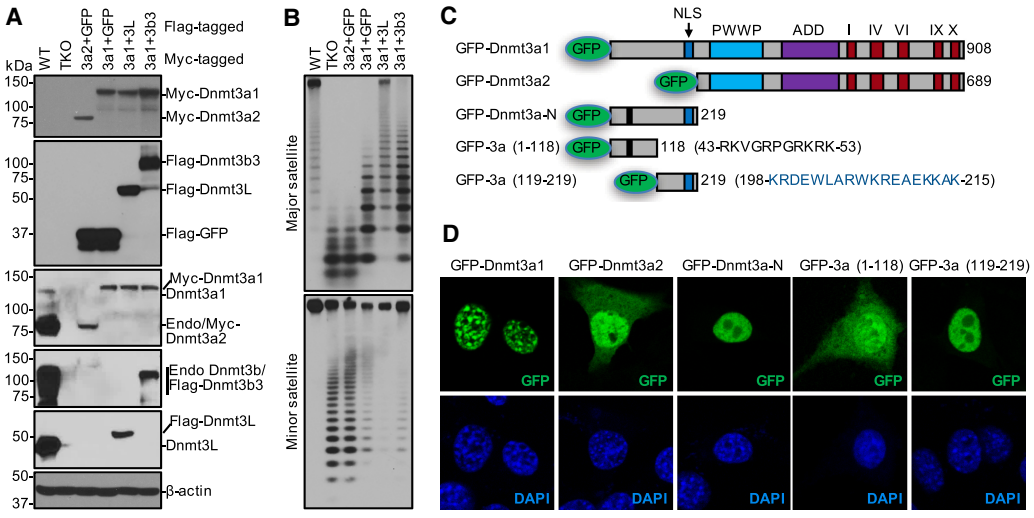

Figure 5. Dnmt3a1 harbors an N-terminal NLS and is active in *Dnmt3a/3b/3l* TKO mESCs. (*A*) Western blots showing the expression of Myc- and FLAG-tagged proteins in stable clones established in *Dnmt3a/3b/3l* TKO mESCs. The Dnmt3a2 + GFP clone was clone 3 in Figure 3. Shown from *top* to *bottom* are blots with Myc, FLAG, Dnmt3a, Dnmt3b, Dnmt3L, and β-actin antibodies. Endo, endogenous. (*B*) Southern blots showing methylation at the major and minor satellite repeats. (*C*) GFP fusion Dnmt3a proteins or fragments used for localization experiment. The two arginine- and lysine-rich sequences in the Dnmt3a1 N-terminal region (Dnmt3a-N) are shown, and the downstream one (residues 198–215) conforms to the consensus sequence of bipartite NLS. (*D*) Images of confocal microscopy showing the typical localization patterns of Dnmt3a proteins or fragments in NIH 3T3 cells, with nuclei being stained with DAPI.

Dnmt3a1 as well, during embryonic development and in somatic cells (Fig. 6).

Previous work indicated that inactive Dnmt3b isoforms can positively or negatively regulate DNA methylation in cancer cell lines (Saito et al. 2002; Weisenberger et al. 2004; Wang et al. 2007; Ostler et al. 2012; Duymich et al. 2016). However, somatic cells, including cancer cell lines, cannot tolerate major changes in DNA methylation, which makes it challenging to investigate how regulators modulate DNA methylation. mESCs are amenable to genetic manipulations and, more importantly, their survival and proliferation are not affected by complete loss of DNA methylation (Tsumura et al. 2006), which offer a unique advantage for dissecting the roles and mechanisms of DNA methylation regulators. Results from our rescue experiments in *Dnmt3a/3b/3l* TKO mESCs clearly show that Dnmt3b3 prefers Dnmt3b over Dnmt3a, although it stimulates Dnmt3a activity to some extent, in agreement with results from a study using the colon cancer line HCT116 (Duymich et al. 2016). However, we cannot rule out the possibility that Dnmt3b3 acts differently in mESCs and cancer cells. Indeed, cancer cells appear to express more DNMT3B isoforms, and some of them may function cooperatively or antagonistically (Ostler et al. 2007, 2012; Duymich et al. 2016).

During the mammalian life cycle, two waves of de novo methylation take place: The first occurs during early embryogenesis, which is mainly catalyzed by Dnmt3b, and the second occurs during germ cell development, which is dependent on Dnmt3a and its accessory factor Dnmt3L (Fig. 6; Okano et al. 1999; Bourc'his et al. 2001; Hata et al. 2002; Kaneda et al. 2004; Borgel et al. 2010). Dnmt3b is also important for DNA methylation in later stages of development and in somatic cells, as deletion of *Dnmt3b* in mouse embryonic fibroblasts results in DNA hypomethylation and genome instability and *DNMT3B* mutations in human are associated with Immunodeficiency, Centromeric instability, and Facial anomalies syndrome, a rare genetic disorder characterized by loss of DNA methylation in heterochromatin regions and defects in antibody production (Dodge et al. 2005; Ehrlich et al. 2008).

The role of Dnmt3L in de novo methylation during embryogenesis has been puzzling. While *Dnmt3l* deficiency results in hypomethylation of some genomic regions, mainly Dnmt3a targets, in early embryos and mESCs (Guenatri et al. 2013; Veland et al. 2019), *Dnmt3l* KO embryos quickly recover their methylation levels (due to increased Dnmt3a expression) and develop normally (Bourc'his et al. 2001; Hata et al. 2002). Although exogenously expressed Dnmt3a, Dnmt3b, and Dnmt3L proteins are capable of interacting with each other (Suetake et al. 2004; Chen et al. 2005; Gowher et al. 2005), it has been reported that endogenous Dnmt3L interacts with Dnmt3a2, but not with Dnmt3a1 and Dnmt3b1, in mESCs (Nimura et al. 2006). This can explain the functional specificity of Dnmt3L. Given that Dnmt3a1 and Dnmt3a2 are equally active in *Dnmt3a/3b* DKO mESCs (Chen et al. 2003), the finding from this study—that Dnmt3a2 has very low activity in *Dnmt3a/3b/3l* TKO mESCs—indicates that an accessory protein is required for Dnmt3a2 function in vivo as a combinational effect of protein stability and protein conformation suitable for engaging in DNA methylation. This observation can explain the nearly identical germline phenotype of mice deficient for Dnmt3L or Dnmt3a2 (which is the predominant isoform of Dnmt3a in germ cells) (Bourc'his et al. 2001; Hata et al. 2002; Bourc'his and Bestor 2004; Kaneda et al. 2004).

Compared with Dnmt3b3 and Dnmt3b6 (Fig. 1A), Dnmt3L lacks the N-terminal region including the PWWP domain, which may contribute to the different potencies of these proteins in stimulating Dnmt3a in cells. Our low-resolution EM models suggest that, in the absence of the N-terminal PWWP domain (which mimics Dnmt3L), the ADD domain of Dnmt3a is in an open conformation (Fig. 2G), while in the presence of the N-terminal PWWP domain, the two copies of the ADD domain

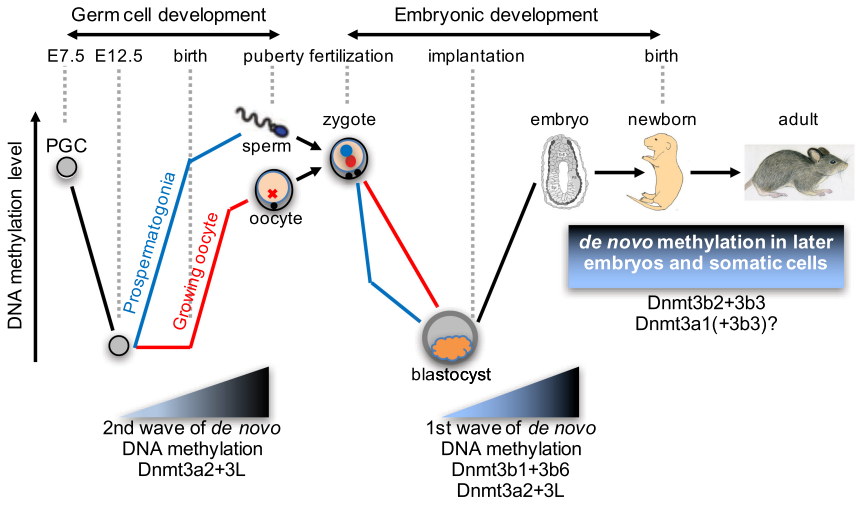

Figure 6. Enzymes and regulators involved in de novo DNA methylation during mouse development. After fertilization, methylation marks inherited from the gametes are mostly erased in paternal (blue) and maternal (red) genomes. After implantation, the first wave of de novo methylation takes place to establish the embryonic methylation pattern. Lower levels of de novo methylation also occur in later stages of development and somatic cells. In early embryos, primordial germ cells (PGCs) undergo another round of demethylation, followed by the second wave de novo methylation to establish sex-specific germ cell methylation patterns. De novo methylation occurs before and after birth in male and female germ cells, respectively. Dnmt3a (predominantly Dnmt3a2) and Dnmt3L are responsible for de novo methylation in germ cells (second wave). Dnmt3b plays a major role and Dnmt3a plays a minor role in de novo methylation during embryonic development.

of Dnmt3a are restrained to the closed conformation (Fig. 2H). We note that the in vitro enzymatic assays were performed with naked DNA oligonucleotides as substrates and the difference between Dnmt3b3 and Dnmt3L in stimulating activities of Dnmt3a2 and Dnmt3b2Δ218 is marginal, 1.7× in Dnmt3a2 (Fig. 1E,F) and 1.1× in Dnmt3b2Δ218 (Supplemental Fig. S1C,D), whereas in cells the DNA methylation is influenced by the chromatin environment including recognition of histone methyl marks at H3K4me0 and H3K36me3 (via ADD and PWWP) and chromosomal DNA binding (via PWWP).

Dnmt3b1 and Dnmt3b6 are highly expressed in early embryos and mESCs (Chen et al. 2002). In differentiated cells, Dnmt3L is silenced, Dnmt3b3 replaces Dnmt3b6 as the major inactive isoform, and Dnmt3b2 replaces Dnmt3b1 as the major active isoform (Chen et al. 2002; Weisenberger et al. 2004). Therefore, the preferences for different enzyme pairs in vivo are likely context dependent. We speculate that the Dnmt3b6-3b1 and Dnmt3L-3a2 complexes are involved in the wave of de novo methylation during early embryogenesis and that the Dnmt3b3-3b2 complex likely plays an important role in carrying out de novo methylation in later stages of development and in somatic cells (Fig. 6). Notably, with the exception of Δ63 deletion in the C-terminal domain, the pair of Dnmt3b1 and Dnmt3b6, and the pair of Dnmt3b2 and Dnmt3b3 have identical amino acid sequence throughout the entire protein including the chromatin-binding PWWP and ADD domains (Supplemental Fig. S1), and thus these pairs are expected to distribute in the same locations within the nuclei and readily form complexes. The availability of proteins for complex formation is likely the major determinant for the preference of Dnmt3b3 for Dnmt3b2 over Dnmt3a1 and 3a2 in cells, as such a preference was not observed in vitro (Fig. 1).

Although Dnmt3a is not essential for embryonic development, *Dnmt3a* KO mice die in several weeks after birth (Okano et al. 1999). Furthermore, somatic *DNMT3A* mutations are frequently observed in acute myeloid leukemia and other hematologic malignancies (Yang et al. 2015). These findings suggest the involvement of Dnmt3a in cellular functions in somatic tissues. Thus, Dnmt3b3 may also assist Dnmt3a1, which is ubiquitously expressed in somatic cells, although Dnmt3a1 is capable of inducing DNA methylation by itself. Our results also suggest that the N-terminal region of Dnmt3a1 is functionally important. We identified a bipartite NLS in the region, which apparently contributes to the exclusive nuclear localization of Dnmt3a1. Based on the different nuclear localization patterns between Dnmt3a1 and Dnmt3a2, the N-terminal region of Dnmt3a1 is also required for heterochromatin enrichment. However, that region alone shows a diffused nuclear localization pattern, suggesting that it is not sufficient but acts together with other regions to target Dnmt3a1 to heterochromatin.

Materials and methods

The plasmids used for protein expression in *Escherichia coli* and mammalian cells are listed in Supplemental Tables S1 and S2, respectively. All antibodies used are listed in Supplemental Table S3.

Protein expression and purification

All plasmids (Supplemental Table S1) were transformed into *Escherichia coli* strain BL21(DE3)-Codon-plus-RIL (Stratagene). Bacterial cells were grown in LB broth at 37°C until reaching $A_{600} \approx 0.6$, the growth temperature was lowered to 16°C and the protein expression was induced with addition of 0.2 mM isopropyl β-D-thiogalactoside overnight. The proteins were purified by three- or four-column chromatography, conducted in a Bio-Rad NGC system, similar to what was described previously (Qiu et al. 2002; Jia et al. 2007; Hashimoto et al. 2012). Briefly, the cell pellets were suspended in lysis buffer of 20 mM Tris-HCl (pH 7.5), 500 mM NaCl, 5% glycerol, and 0.5 mM Tris (2-carboxyethyl) phosphine (TCEP) and the purified proteins were stocked at −80°C in the storage buffer of 20 mM Tris-HCl (pH 7.5), 150 mM NaCl, 5% glycerol, and 0.5 mM TCEP.

For His-tagged Dnmt3a2 (pXC465) and Dnmt3b2Δ218 (pXC273) and His-sumo-tagged Dnmt3b3Δ218 (pXC1048), three columns from GE Healthcare, HisTrap HP, HiTrap Heparin HP, and HiLoad 16/60 Superdex 200 were used. His-sumo tag was cleaved by ULP1 (produced in-house).

The complex of His-Dnmt3a2 (pXC465) and GST-Dnmt 3b3Δ218 (pXC1044) was obtained using colysis and two affinity columns: HisTrap HP and Glutathione Sepharose 4B. GST tag was removed with PreScission protease (produced in-house). The complex was further purified by HiTrap Heparin HP and Superdex 200 increase 10/300 GL.

For the ΔPWWP complex of His-sumo-Dnmt3a2 (residues 421–908; pXC531) and GST-Dnmt3b3 (residues 387–776; pXC1032), the supernatant of colysate was passing through glutathione sepharose 4B and HisTrap HP. The His-sumo tag and GST tag were removed by ubiquitin-like-specific protease ULP1 and PreScission protease, respectively. The complex was further purified by HiTrap Q HP and Superdex 200 increase 10/300 GL.

In vitro DNA methylation assay

The methyl transfer activity assays were performed using the Promega bioluminescence assay (MTase-Glo) (Hsiao et al. 2016). The assay measures the methylation reaction by-product SAH, which is converted into ATP in a two-step reaction, and ATP was detected through a luciferase assay. The reaction in 30-μL volume contained 25 μM SAM, 5 μM substrate DNA (Fig. 1), and 0.5 μM individual protein or protein complex in 20 mM Tris-HCl (pH 7.5), 20% glycerol, 4 mM DTT, and 40 mM NaCl at 37°C. The individual protein or protein complex was preincubated with SAM for 5 min at room temperature before the addition of DNA. An aliquot of 10 μL of sample was taken from the reaction mixture and 0.1% (v/v) trifluoroacetic acid was added to stop the reaction. A 5-μL of reaction sample was transferred to a low-volume 384-well plate and the luminescence assay was performed according to the manufacturer's protocol. A Synergy 4 multimode microplate reader (BioTek) was used to measure luminescence signal. The kinetics measurements were performed for 1 h at 37°C with a total volume of 10 μL and varying concentration of substrate DNA.

Size exclusion chromatography coupled to multiangle light scattering (SEC-MALS)

Multiangle light-scattering (MALS) experiments were performed using an 18-angle DAWN HELEOS II light-scattering detector

connected in tandem to an Optilab refractive index concentration detector (Wyatt Technology) and coupled to a Shodex KW803 column. Bovine serum albumin (BSA; 45-µL sample at 10 mg/mL) in the same SEC running buffer (20 mM Tris at pH 7.5, 150 mM NaCl and 1 mM β-mercaptoethanol) was used for system normalization and calibration. The UV absorbance of each sample was recorded at 280 and 260 nm simultaneously. The samples (Dnmt3a2-3b3Δ218 complex [5 mg/mL and 10 mg/mL] and Dnmt3a2-3b3 [ΔPWWP] complex [8 mg/mL]) in the same SEC running buffer were injected into the Shodex KW803 column. The UV, MALS, and differential refractive index data were analyzed using Wyatt Astra 7 software to monitor the homogeneity of the sample across the elution peak and determine the molar mass of the purified protein–protein complexes.

Size exclusion chromatography coupled to small angle X-ray scattering (SEC-SAXS)

SAXS data were collected in line with MALS. A total of 60 µL of each sample containing Dnmt3a2-3b3Δ218 complex (5 mg/mL and 10 mg/mL) and Dnmt3a2-3b3 (ΔPWWP) complex (8 mg/mL) was prepared in SEC running buffer. Inline SEC-SAXS was performed using an online Agilent 1260 Infinity HPLC system equipped with a Shodex KW803 column. The column was equilibrated with running buffer with a flow rate of 0.4 mL/min. All experiments were performed at 20°C and the SAXS data were collected at ALS beamline 12.3.1 (Dyer et al. 2014) and were processed as described (Hura et al. 2009). The program SCÅTTER was used for primary reduction of the SAXS data and for further data processing to obtain the radius of gyration (Rg), the maximum particle dimension (Dmax), the excluded particle volume (Vp) and the pair wise distribution function [P(r)]. The molecular weight of the purified complexes was calculated using the protocol described (Rambo and Tainer 2013). The initial low-resolution 3D ab initio models were generated by DAMMIF (Franke and Svergun 2009), which were later averaged and filtered with DAMAVER and DAMFILT (Volkov and Svergun 2003). Structural visualization, analysis, and figure preparation were performed using PyMol (Schrödinger, LLC) and UCSF Chimera (Pettersen et al. 2004).

Sedimentation velocity-analytical ultracentrifugation (SV-AUC)

Purified Dnmt3a2/3b3Δ218 complex (~1 mg/mL) was dialyzed in 20 mM Tris (pH 7.5), 150 mM NaCl, and 1 mM DTT overnight at 4°C. A Beckman-Coulter XL-A equipped with a TiAn50 eight-hole rotor with two-channel epon centerpiece (12 mm) and quartz window was used to carry out SV-AUC experiments. The absorbance scans were monitored at 280 nm every 1-min interval at 40,000 rpm for ~6 h at 4°C. The solvent density (ρ) and viscosity (η) of the chemical components present in the buffer were calculated using Sednterp (Alliance Protein Laboratories). To analyze the collected AUC data, the continuous distribution c(s) model was selected, and data were analyzed using the program Sedfit (Schuck 2000).

Negative stain transmission electron microscopy (EM)

The specimens were prepared using conventional negative staining procedure. Briefly, 3 µL of each purified protein complex (Dnmt3a2-3b3Δ218 at 0.03 mg/mL, Dnmt3a2-3b3 [ΔPWWP] at ~0.0125 mg/mL and the C-terminal minimal domain complex at 0.05 mg/mL) were adsorbed onto a glow discharged carbon-coated grids (CF200-CU; EMS) for 60 sec. The EM grids were blotted with Whatman's filter paper 541 and washed with two consecutive drops of deionized water (20 µL each) with blotting excess liquid in between subsequent washes. The EM grids were further stained with three consecutive drops of uranyl acetate (2%) or uranyl formate (1%) solution, blotted to remove residual stain and air-dried in the fume hood.

The negative stained grids were imaged at room temperature using a JEM 2100 transmission electron microscope operated at 200 keV (JOEL) equipped with a LaB6 filament, 3kx4k Direct Electron Detector (DE12) and a Gatan 4kx4k CCD at the EM core facility of the Baylor college of Medicine. The images were recorded between 20,000× and 40,000× using low-dose procedures and a defocus range of −1 to −4 µm. All the steps of image processing (CTF estimation, initial particle picking, particle extraction, 2D classification, ab initio 3D models, and homogeneous refinement with C2 symmetry) were carried out using cryoSPARC (Punjani et al. 2017). A total of 8056, 5612, and 5845 particles, respectively, were picked manually for the C-terminal minimal domain complex, Dnmt3a2-3b3Δ218 and Dnmt3a2-3b3ΔPWWP samples. The generated 3D EM maps were visualized using UCSF Chimera software package (Pettersen et al. 2004). The available X-ray structures of Dnmt3a-3L C-terminal domain complex (PDB 2QRVand 4U7P) and ADD of Dnmt3a (PDB 3A1A) and PWWP domain of Dnmt3b (PDB 1KHC and 5CIU) were docked into the generated EM maps or SAXS-derived dummy atom models using the "fit in map" command of Chimera.

mESC culture and generation of stable clones

mESCs were maintained on gelatin-coated petri dishes in serum-containing medium (DMEM supplemented with 15% fetal bovine serum, 0.1 mM nonessential amino acids, 0.1 mM β-mercaptoethanol, 50 U/mL penicillin, 50 µg/mL streptomycin, 10^3 U/mL leukemia inhibitory factor). Generation of stable clones in mESCs were described previously (Chen et al. 2003; Kim et al. 2013; Veland et al. 2019). Briefly, plasmids expressing Myc- and FLAG-tagged proteins simultaneously were transfected into *Dnmt3a/3b* DKO or *Dnmt3a/3b/3l* TKO mESCs using Lipofectamine 2000 (Invitrogen), then seeded at low density in dishes coated with feeder cells, selected with Blasticidin S HCl (Gibco) for 7 d, and individual clones were picked. Protein expression was analyzed by Western blotting with antibodies (Supplemental Table S3).

Southern blot and dot blot

DNA methylation at the major and minor satellite repeats were analyzed by Southern blot after digestion of genomic DNA with methylation-sensitive restriction enzymes (MaeII for major satellite, HpaII for minor satellite) as described previously (Chen et al. 2003; Kim et al. 2013; Veland et al. 2019). Detection was performed using biotin-labeled probes and the North2South chemiluminescent hybridization and detection kit (Thermo Fisher Scientific). Total 5mC levels were analyzed by dot blot as described previously (Dan et al. 2017). Briefly, genomic DNA was denatured in 0.4 N NaOH and 10 mM EDTA for 10 min at 95°C and twofold serial dilutions were spotted on positively charged nylon membranes. The membranes were immuoblotted with 5mC antibody. DNA loading was verified by staining with SYTOX Green.

Bisulfite sequencing

Bisulfite sequencing analysis of the methylation levels at IAP retrotransposons was carried out as described previously (Veland et al. 2019). Briefly, genomic DNA was treated for bisulfite

conversion using the EZ DNA methylation kit (Zymo Research) and then used as template to amplify an IAP region with eight to 12 CpG dinucleotides (due to sequence variations) using the following primers: 5′-CACGGATCCTTGTGTTTTAAGTGGT AAATAAAT-3′ (CT-462, F) and 5′-GTCGAATTCAAAAAAAAC ACACAAACCAAAAT-3′ (CT-464, R). PCR products were digested with BamHI-EcoRI (restriction sites are underlined) and cloned into pBluescript SK (Stratagene). For each sample, multiple clones were sequenced.

CRISPR/Cas9 gene editing

Gene targeting by CRISPR/Cas9 was performed as described previously (Hardikar et al. 2020). *Dnmt3a/3b/3l* TKO mESCs were generated by disrupting *Dnmt3l* in late-passage *Dnmt3a/3b* DKO mESCs (Okano et al. 1999). Briefly, a synthesized gBlock (Integrated DNA Technologies) containing the sequence for U6 promoter-driven *Dnmt3l* sgRNA (in exon 6) was cotransfected with the *pCAG-Cas9-IRES-GFP* vector, and GFP-positive cells were sorted 24 h after transfection and seeded at low density in dishes coated with feeder cells to derive individual clones. Mutant clones were identified by DNA sequencing and verified by Western blotting.

Coimmunoprecipitation

To verify protein–protein interactions, Myc-tagged Dnmt3a2 or Dnmt3b2 and HA-tagged Dnmt3b3 or its F659D substitution were transiently expressed in HEK293 cells or *Dnmt3a/3b/3l* TKO mESCs. Twenty-four hours after transfection, the cells were lysed in lysis buffer (20 mM Tris–HCl at pH 7.9, 150 mM NaCl, 0.1% NP-40, 1 mM EDTA, 3 mM $MgCl_2$, 10% glycerol, 1× protease inhibitor cocktail [Thermo Scientific]), and IP was performed using Protein A/G UltraLink resin beads (Thermo Fisher Scientific). Total cell lysates (input) and IP samples were analyzed by Western blotting with Myc and HA antibodies.

Protein localization

Plasmids expressing GFP-Dnmt3a proteins or fragments or GFP-Dnmt3b-N were transiently transfected into NIH3T3 cells plated on glass coverslips. Twenty-four hours after transfection, the cells were fixed with 3.7% paraformaldehyde, and nuclei were stained with 4′,6-diamidino-2-phenylindole (DAPI). The slides were viewed and imaged with confocal microscopy.

Acknowledgments

We thank Dr. Yiwei Liu for his initial work in preparing expression constructs, protein purifications, and activity assays; Dr. Zhongwu Zhou for his participation of EM examination; Dr. Anup Kumar Singh, Dr. Jiameng Dan, Dr. Nicolas Veland, Dr. Tewfik Hamidi, and Dr. Bigang Liu for discussions and technical assistance; and Ms. Yu Cao for technical assistance. We thank Dr. B.V. Venkatar Prasad and Dr. Soni Kaundal at Baylor College of Medicine for help in sedimentation velocity analytical ultracentrifugation experiments. This work is supported by the U.S. National Institutes of Health (NIH; R35GM134744 to X.C. and R01AI1214030A1 to T.C.), the Cancer Prevention and Research Institute of Texas (CPRIT; RR160029 to X.C., who is a CPRIT Scholar in Cancer Research), a Thomas Endowment fellowship (to Y.Z.), and a Sam and Freda Davis Fund fellowship (to Z.Y.). NIH P30GM124169-01 and the Department of Energy's Office of Biological and Environmental Research Integrated Diffraction Analysis Technology Program support SAXS data collection at SIBYLS. CPRIT RP190602 partially supports the CryoEM/CryoET Core at Baylor College of Medicine. CPRIT RP170628 partially supports confocal microscopy.

Authors contributions: Y.Z. generated mESC lines and performed rescue experiments. R.R. performed protein expression, purification, and activity assays. G.K. performed biophysical experiments. S.H. and L.B. generated plasmid constructs and performed localization and bisulfite sequencing experiments. Z.Y. performed dot blots. E.G. participated in mESC culture and DNA methylation analysis. X.Z. participated in discussion throughout the project. X.C. conceived the initial concept. T.C. and X.C organized and designed the scope of the study and prepared the manuscript.

References

Abyzov A, Vaccarino FM. 2020. Cell lineage tracing and cellular diversity in humans. *Annu Rev Genomics Hum Genet* **21:** 101–116. doi:10.1146/annurev-genom-083118-015241

Anteneh H, Fang J, Song J. 2020. Structural basis for impairment of DNA methylation by the DNMT3A R882H mutation. *Nat Commun* **11:** 2294. doi:10.1038/s41467-020-16213-9

Bestor TH. 2000. The DNA methyltransferases of mammals. *Hum Mol Genet* **9:** 2395–2402. doi:10.1093/hmg/9.16.2395

Borgel J, Guibert S, Li Y, Chiba H, Schübeler D, Sasaki H, Forné T, Weber M. 2010. Targets and dynamics of promoter DNA methylation during early mouse development. *Nat Genet* **42:** 1093–1100. doi:10.1038/ng.708

Bourc'his D, Bestor TH. 2004. Meiotic catastrophe and retrotransposon reactivation in male germ cells lacking Dnmt3L. *Nature* **431:** 96–99. doi:10.1038/nature02886

Bourc'his D, Xu GL, Lin CS, Bollman B, Bestor TH. 2001. Dnmt3L and the establishment of maternal genomic imprints. *Science* **294:** 2536–2539. doi:10.1126/science.1065848

Chedin F, Lieber MR, Hsieh CL. 2002. The DNA methyltransferase-like protein DNMT3L stimulates de novo methylation by Dnmt3a. *Proc Natl Acad Sci* **99:** 16916–16921. doi:10.1073/pnas.262443999

Chen T, Ueda Y, Xie S, Li E. 2002. A novel Dnmt3a isoform produced from an alternative promoter localizes to euchromatin and its expression correlates with active de novo methylation. *J Biol Chem* **277:** 38746–38754. doi:10.1074/jbc.M205312200

Chen T, Ueda Y, Dodge JE, Wang Z, Li E. 2003. Establishment and maintenance of genomic methylation patterns in mouse embryonic stem cells by Dnmt3a and Dnmt3b. *Mol Cell Biol* **23:** 5594–5605. doi:10.1128/MCB.23.16.5594-5605.2003

Chen T, Tsujimoto N, Li E. 2004. The PWWP domain of Dnmt3a and Dnmt3b is required for directing DNA methylation to the major satellite repeats at pericentric heterochromatin. *Mol Cell Biol* **24:** 9048–9058. doi:10.1128/MCB.24.20.9048-9058.2004

Chen ZX, Mann JR, Hsieh CL, Riggs AD, Chédin F. 2005. Physical and functional interactions between the human DNMT3L protein and members of the de novo methyltransferase family. *J Cell Biochem* **95:** 902–917. doi:10.1002/jcb.20447

Cheng X, Blumenthal RM. 2010. Coordinated chromatin control: structural and functional linkage of DNA and histone methylation. *Biochemistry* **49:** 2999–3008. doi:10.1021/bi100213t

Dan J, Rousseau P, Hardikar S, Veland N, Wong J, Autexier C, Chen T. 2017. Zscan4 inhibits maintenance DNA methylation to facilitate telomere elongation in mouse embryonic

stem cells. *Cell Rep* **20:** 1936–1949. doi:10.1016/j.celrep.2017.07.070

De Carvalho DD, You JS, Jones PA. 2010. DNA methylation and cellular reprogramming. *Trends Cell Biol* **20:** 609–617. doi:10.1016/j.tcb.2010.08.003

Dhayalan A, Rajavelu A, Rathert P, Tamas R, Jurkowska RZ, Ragozin S, Jeltsch A. 2010. The Dnmt3a PWWP domain reads histone 3 lysine 36 trimethylation and guides DNA methylation. *J Biol Chem* **285:** 26114–26120. doi:10.1074/jbc.M109.089433

Dodge JE, Okano M, Dick F, Tsujimoto N, Chen T, Wang S, Ueda Y, Dyson N, Li E. 2005. Inactivation of Dnmt3b in mouse embryonic fibroblasts results in DNA hypomethylation, chromosomal instability, and spontaneous immortalization. *J Biol Chem* **280:** 17986–17991. doi:10.1074/jbc.M413246200

Duymich CE, Charlet J, Yang X, Jones PA, Liang G. 2016. DNMT3B isoforms without catalytic activity stimulate gene body methylation as accessory proteins in somatic cells. *Nat Commun* **7:** 11453. doi:10.1038/ncomms11453

Dyer KN, Hammel M, Rambo RP, Tsutakawa SE, Rodic I, Classen S, Tainer JA, Hura GL. 2014. High-throughput SAXS for the characterization of biomolecules in solution: a practical approach. *Methods Mol Biol* **1091:** 245–258. doi:10.1007/978-1-62703-691-7_18

Ehrlich M, Sanchez C, Shao C, Nishiyama R, Kehrl J, Kuick R, Kubota T, Hanash SM. 2008. ICF, an immunodeficiency syndrome: DNA methyltransferase 3B involvement, chromosome anomalies, and gene dysregulation. *Autoimmunity* **41:** 253–271. doi:10.1080/08916930802024202

Ferrer AI, Trinidad JR, Sandiford O, Etchegaray JP, Rameshwar P. 2020. Epigenetic dynamics in cancer stem cell dormancy. *Cancer Metastasis Rev* **39:** 721–738. doi: 10.1007/s10555-020-09882-x.

Franke D, Svergun DI. 2009. DAMMIF, a program for rapid ab-initio shape determination in small-angle scattering. *J Appl Crystallogr* **42:** 342–346. doi:10.1107/S0021889809000338

Gao L, Emperle M, Guo Y, Grimm SA, Ren W, Adam S, Uryu H, Zhang ZM, Chen D, Yin J, et al. 2020. Comprehensive structure–function characterization of DNMT3B and DNMT3A reveals distinctive de novo DNA methylation mechanisms. *Nat Commun* **11:** 3355. doi:10.1038/s41467-020-17109-4

Goll MG, Bestor TH. 2005. Eukaryotic cytosine methyltransferases. *Annu Rev Biochem* **74:** 481–514. doi:10.1146/annurev.biochem.74.010904.153721

Gowher H, Liebert K, Hermann A, Xu G, Jeltsch A. 2005. Mechanism of stimulation of catalytic activity of Dnmt3A and Dnmt3B DNA-(cytosine-C5)-methyltransferases by Dnmt3L. *J Biol Chem* **280:** 13341–13348. doi:10.1074/jbc.M413412200

Guenatri M, Duffie R, Iranzo J, Fauque P, Bourc'his D. 2013. Plasticity in Dnmt3L-dependent and -independent modes of de novo methylation in the developing mouse embryo. *Development* **140:** 562–572. doi:10.1242/dev.089268

Guo X, Wang L, Li J, Ding Z, Xiao J, Yin X, He S, Shi P, Dong L, Li G, et al. 2015. Structural insight into autoinhibition and histone H3-induced activation of DNMT3A. *Nature* **517:** 640–644. doi:10.1038/nature13899

Hardikar S, Ying Z, Zeng Y, Zhao H, Liu B, Veland N, McBride K, Cheng X, Chen T. 2020. The ZBTB24–CDCA7 axis regulates HELLS enrichment at centromeric satellite repeats to facilitate DNA methylation. *Protein Cell* **11:** 214–218. doi:10.1007/s13238-019-00682-w

Hashimoto H, Liu Y, Upadhyay AK, Chang Y, Howerton SB, Vertino PM, Zhang X, Cheng X. 2012. Recognition and potential mechanisms for replication and erasure of cytosine hydroxymethylation. *Nucleic Acids Res* **40:** 4841–4849. doi:10.1093/nar/gks155

Hata K, Okano M, Lei H, Li E. 2002. Dnmt3L cooperates with the Dnmt3 family of de novo DNA methyltransferases to establish maternal imprints in mice. *Development* **129:** 1983–1993.

Hsiao K, Zegzouti H, Goueli SA. 2016. Methyltransferase-Glo: a universal, bioluminescent and homogenous assay for monitoring all classes of methyltransferases. *Epigenomics* **8:** 321–339. doi:10.2217/epi.15.113

Hura GL, Menon AL, Hammel M, Rambo RP, Poole FL 2nd, Tsutakawa SE, Jenney FE Jr, Classen S, Frankel KA, Hopkins RC, et al. 2009. Robust, high-throughput solution structural analyses by small angle X-ray scattering (SAXS). *Nat Methods* **6:** 606–612. doi:10.1038/nmeth.1353

Jia D, Jurkowska RZ, Zhang X, Jeltsch A, Cheng X. 2007. Structure of Dnmt3a bound to Dnmt3L suggests a model for de novo DNA methylation. *Nature* **449:** 248–251. doi:10.1038/nature06146

Jones PA, Baylin SB. 2002. The fundamental role of epigenetic events in cancer. *Nat Rev Genet* **3:** 415–428. doi:10.1038/nrg816

Jones PA, Liang G. 2009. Rethinking how DNA methylation patterns are maintained. *Nat Rev Genet* **10:** 805–811. doi:10.1038/nrg2651

Kaneda M, Okano M, Hata K, Sado T, Tsujimoto N, Li E, Sasaki H. 2004. Essential role for de novo DNA methyltransferase Dnmt3a in paternal and maternal imprinting. *Nature* **429:** 900–903. doi:10.1038/nature02633

Kareta MS, Botello ZM, Ennis JJ, Chou C, Chédin F. 2006. Reconstitution and mechanism of the stimulation of de novo methylation by human DNMT3L. *J Biol Chem* **281:** 25893–25902. doi:10.1074/jbc.M603140200

Kikhney AG, Svergun DI. 2015. A practical guide to small angle X-ray scattering (SAXS) of flexible and intrinsically disordered proteins. *FEBS Lett* **589:** 2570–2577. doi:10.1016/j.febslet.2015.08.027

Kim SJ, Zhao H, Hardikar S, Singh AK, Goodell MA, Chen T. 2013. A DNMT3A mutation common in AML exhibits dominant-negative effects in murine ES cells. *Blood* **122:** 4086–4089. doi:10.1182/blood-2013-02-483487

Kosugi S, Hasebe M, Matsumura N, Takashima H, Miyamoto-Sato E, Tomita M, Yanagawa H. 2009. Six classes of nuclear localization signals specific to different binding grooves of importin α. *J Biol Chem* **284:** 478–485. doi:10.1074/jbc.M807017200

Li E, Zhang Y. 2014. DNA methylation in mammals. *Cold Spring Harb Perspect Biol* **6:** a019133. doi:10.1101/cshperspect.a019133

Lin CC, Chen YP, Yang WZ, Shen JCK, Yuan HS. 2020. Structural insights into CpG-specific DNA methylation by human DNA methyltransferase 3B. *Nucleic Acids Res* **48:** 3949–3961. doi:10.1093/nar/gkaa111

Lyko F. 2018. The DNA methyltransferase family: a versatile toolkit for epigenetic regulation. *Nat Rev Genet* **19:** 81–92. doi:10.1038/nrg.2017.80

Nimura K, Ishida C, Koriyama H, Hata K, Yamanaka S, Li E, Ura K, Kaneda Y. 2006. Dnmt3a2 targets endogenous Dnmt3L to ES cell chromatin and induces regional DNA methylation. *Genes Cells* **11:** 1225–1237. doi:10.1111/j.1365-2443.2006.01012.x

Okano M, Xie S, Li E. 1998. Cloning and characterization of a family of novel mammalian DNA (cytosine-5) methyltransferases. *Nat Genet* **19:** 219–220. doi:10.1038/890

Okano M, Bell DW, Haber DA, Li E. 1999. DNA methyltransferases Dnmt3a and Dnmt3b are essential for de novo

methylation and mammalian development. *Cell* **99:** 247–257. doi:10.1016/S0092-8674(00)81656-6

Ooi SKT, Qiu C, Bernstein E, Li K, Jia D, Yang Z, Erdjument-Bromage H, Tempst P, Lin S-P, Allis CD, et al. 2007. DNMT3L connects unmethylated lysine 4 of histone H3 to de novo methylation of DNA. *Nature* **448:** 714–717. doi:10.1038/nature05987

Ostler KR, Davis EM, Payne SL, Gosalia BB, Expósito-Céspedes J, Le Beau MM, Godley LA. 2007. Cancer cells express aberrant DNMT3B transcripts encoding truncated proteins. *Oncogene* **26:** 5553–5563. doi:10.1038/sj.onc.1210351

Ostler KR, Yang Q, Looney TJ, Zhang L, Vasanthakumar A, Tian Y, Kocherginsky M, Raimondi SL, DeMaio JG, Salwen HR, et al. 2012. Truncated DNMT3B isoform DNMT3B7 suppresses growth, induces differentiation, and alters DNA methylation in human neuroblastoma. *Cancer Res* **72:** 4714–4723. doi:10.1158/0008-5472.CAN-12-0886

Otani J, Nankumo T, Arita K, Inamoto S, Ariyoshi M, Shirakawa M. 2009. Structural basis for recognition of H3K4 methylation status by the DNA methyltransferase 3A ATRX–DNMT3–DNMT3L domain. *EMBO Rep* **10:** 1235–1241. doi:10.1038/embor.2009.218

Pettersen EF, Goddard TD, Huang CC, Couch GS, Greenblatt DM, Meng EC, Ferrin TE. 2004. UCSF chimera–a visualization system for exploratory research and analysis. *J Comput Chem* **25:** 1605–1612. doi:10.1002/jcc.20084

Punjani A, Rubinstein JL, Fleet DJ, Brubaker MA. 2017. cryoSPARC: algorithms for rapid unsupervised cryo-EM structure determination. *Nat Methods* **14:** 290–296. doi:10.1038/nmeth.4169

Qiu C, Sawada K, Zhang X, Cheng X. 2002. The PWWP domain of mammalian DNA methyltransferase Dnmt3b defines a new family of DNA-binding folds. *Nat Struct Biol* **9:** 217–224.

Rambo RP, Tainer JA. 2013. Accurate assessment of mass, models and resolution by small-angle scattering. *Nature* **496:** 477–481. doi:10.1038/nature12070

Robertson KD, Uzvolgyi E, Liang G, Talmadge C, Sumegi J, Gonzales FA, Jones PA. 1999. The human DNA methyltransferases (DNMTs) 1, 3a and 3b: coordinate mRNA expression in normal tissues and overexpression in tumors. *Nucleic Acids Res* **27:** 2291–2298. doi:10.1093/nar/27.11.2291

Saito Y, Kanai Y, Sakamoto M, Saito H, Ishii H, Hirohashi S. 2002. Overexpression of a splice variant of DNA methyltransferase 3b, DNMT3b4, associated with DNA hypomethylation on pericentromeric satellite regions during human hepatocarcinogenesis. *Proc Natl Acad Sci* **99:** 10060–10065. doi:10.1073/pnas.152121799

Sakai Y, Suetake I, Shinozaki F, Yamashina S, Tajima S. 2004. Co-expression of de novo DNA methyltransferases Dnmt3a2 and Dnmt3L in gonocytes of mouse embryos. *Gene Expr Patterns* **5:** 231–237. doi:10.1016/j.modgep.2004.07.011

Schuck P. 2000. Size-distribution analysis of macromolecules by sedimentation velocity ultracentrifugation and lamm equation modeling. *Biophys J* **78:** 1606–1619. doi:10.1016/S0006-3495(00)76713-0

Some D, Amartely H, Tsadok A, Lebendiker M. 2019. Characterization of proteins by size-exclusion chromatography coupled to multi-angle light scattering (SEC-MALS). *J Vis Exp* **148:** e59615.

Suetake I, Shinozaki F, Miyagawa J, Takeshima H, Tajima S. 2004. DNMT3L stimulates the DNA methylation activity of Dnmt3a and Dnmt3b through a direct interaction. *J Biol Chem* **279:** 27816–27823. doi:10.1074/jbc.M400181200

Tsumura A, Hayakawa T, Kumaki Y, Takebayashi S, Sakaue M, Matsuoka C, Shimotohno K, Ishikawa F, Li E, Ueda HR, et al. 2006. Maintenance of self-renewal ability of mouse embryonic stem cells in the absence of DNA methyltransferases Dnmt1, Dnmt3a and Dnmt3b. *Genes Cells* **11:** 805–814. doi:10.1111/j.1365-2443.2006.00984.x

Veland N, Lu Y, Hardikar S, Gaddis S, Zeng Y, Liu B, Estecio MR, Takata Y, Lin K, Tomida MW, et al. 2019. DNMT3L facilitates DNA methylation partly by maintaining DNMT3A stability in mouse embryonic stem cells. *Nucleic Acids Res* **47:** 152–167. doi:10.1093/nar/gky947

Volkov VV, Svergun DI. 2003. Uniqueness of *ab initio* shape determination in small-angle scattering. *J Appl Crystallogr* **36:** 860–864. doi:10.1107/S0021889803000268

Wang J, Bhutani M, Pathak AK, Lang W, Ren H, Jelinek J, He R, Shen L, Issa JP, Mao L. 2007. *ΔDNMT3B* variants regulate DNA methylation in a promoter-specific manner. *Cancer Res* **67:** 10647–10652. doi:10.1158/0008-5472.CAN-07-1337

Webster KE, O'Bryan MK, Fletcher S, Crewther PE, Aapola U, Craig J, Harrison DK, Aung H, Phutikanit N, Lyle R, et al. 2005. Meiotic and epigenetic defects in Dnmt3L-knockout mouse spermatogenesis. *Proc Natl Acad Sci* **102:** 4068–4073. doi:10.1073/pnas.0500702102

Weinberg DN, Papillon-Cavanagh S, Chen H, Yue Y, Chen X, Rajagopalan KN, Horth C, McGuire JT, Xu X, Nikbakht H, et al. 2019. The histone mark H3K36me2 recruits DNMT3A and shapes the intergenic DNA methylation landscape. *Nature* **573:** 281–286. doi:10.1038/s41586-019-1534-3

Weisenberger DJ, Velicescu M, Cheng JC, Gonzales FA, Liang G, Jones PA. 2004. Role of the DNA methyltransferase variant DNMT3b3 in DNA methylation. *Mol Cancer Res* **2:** 62–72.

Westerman KE, Ordovás JM. 2020. DNA methylation and incident cardiovascular disease. *Curr Opin Clin Nutr Metab Care* **23:** 236–240. doi:10.1097/MCO.0000000000000659

Xu T, Liu M, Zhou XE, Liang G, Zhao G, Xu HE, Melcher K, Jones PA. 2020. Structure of nucleosome-bound DNA methyltransferases DNMT3A and DNMT3B. *Nature* **586:** 151–155. doi:10.1038/s41586-020-2747-1

Yang L, Rau R, Goodell MA. 2015. DNMT3A in haematological malignancies. *Nat Rev Cancer* **15:** 152–165. doi:10.1038/nrc3895

Zhang ZM, Lu R, Wang P, Yu Y, Chen D, Gao L, Liu S, Ji D, Rothbart SB, Wang Y, et al. 2018. Structural basis for DNMT3A-mediated de novo DNA methylation. *Nature* **554:** 387–391. doi:10.1038/nature25477